Research Article

# DESIGN OF WRAPAROUND MICROSTRIP ANTENNA USING THE METHOD OF MOMENT

Alnawars Mohammed[1], Wa'il A. Godaymi Al-Tumah[2], Ra'ed Malallah[3*]

[1,2,3]*Department of Physics, Faculty of Science, University of Basrah, Garmat Ali, Basrah, 61004, Iraq*

**\*Corresponding Author email:** raed.malallah@ucdconnect.ie

## ABSTRACT

*Wrapped antennas are described as the omnidirectional coverage antennas, thus it has been discussed in wide studies. In this study shows how to calculate the radiation pattern for a wraparound microstrip antenna by solving the integral equation of the electric and magnetic fields. The modelling has been done by representing the body with regular geometrical shape such as a Body of Revolution (BoR). The wraparound microstrip antenna is considered as a conducing cylinder patch which be uniformly coated around a lossless dielectric having dielectric constant. Both are substrates around a conducing cylinder as ground patch. Analytically the prediction results have been calculated using the Method of Moment (MoM). It is worth noting that these predictions are in a good qualitative agreement with previous studies. We also has been examined the case involving two simultaneous patches using the electromagnetic boundary conditions to solve the differential and integral equations. These types of antennas are used in many applications such as medical, military as in the rockets, etc.*

## INTRODUCTION

The microstrip antennas are preferred over other antennas because it has the ability to correspond with different surfaces, especially with high-speed vehicles such as aircraft and missiles (1). As a brief historical review, *Munson* presented a study of the wraparound microstrip antenna in 1972, which led to his rise in popularity. That the radiators used by *Munson* are metal strips wrapped around missiles (2). Radiation pattern has also been obtained of a wraparound microstrip antenna in 1983 by *Fonseca* and *Giarola*. They used the Green Function when the medium is in the form of concentric layers, then demonstrated that the radiation pattern operating at 2 GHz does not depend very much on the antenna diameters (3). In 2009, *Venture*, used the MoM technique that to analyze a wraparound microstrip antenna through and predictions the results of radiation pattern and input resistance. Where they showed, in order to achieve an omnidirectional pattern, the spacing between probes should be no exceed than $\lambda_d$ (4).

The wraparound microstrip antennas consist of an inner cavity of a typical cylindrical electrical conductor with a radius *a*, surrounded by a dielectric substrate, which is having a dielectric constant $\epsilon_r$ and thickness *h*. The antenna length is usually

expressed as a half wavelength. As well as that the small rings (representing the patches) are placed over the dielectric which has a width equal a half wavelength in the dielectric substrate, $\lambda_d/2$. That one is located between the conductor and the patch, where the patch width is $\lambda_\circ/\sqrt{\epsilon_r}$ (5).

The purpose of this study is to provide a detailed analysis of wraparound microstrip antennas in order to find radiation patterns by using the principle of equivalence and the method of moment which is one of the numerical methods with high accuracy analysis. We proposed that the antenna is fed by four orthogonal dipoles that allowing the antenna to radiate an omnidirectional pattern (6). It is worth mentioning that the MoM was used to determine the equivalent currents as the electrical surface currents on the wraparound microstrip antenna patch, which are equivalent to the magnetic currents that surround the patch within the insulating substrate which produces magnetic fields.

## NUMERICAL ANALYSIS:

Antennas and their design methods are among the most important applications that are used in our life, as they mainly depends on electromagnetic theory. To solve any electromagnetic problem is theoretically represented, using a one of the analytical and numerical models. Among the analytical models used, the main focus of this research on MoM, due to its wide features, especially the applications using the body of revolution (BoR) (7) (8). This type of antenna has several applications, and the most important of which is in the military applications "such as missiles". To proceed numerically, we select the wraparound antenna that has been represented in Fig. 1, which fed by four dipoles for an omnidirectional radiation pattern in 433MHz. As can be seen in this figure, the single patch wraparound antenna contains from of three overlapping cylinders. The inner one is made from conductive material and named the ground-plane, which coated by a homogeneous dielectric-substrate (where the dielectric permittivity is $\epsilon_r = 2.32$). Then, the conductor cylinder patch is covered the waist of outer dielectric-substrate, which is the important part of the antenna. It is worth noting that the most of antenna measured parameters depends on the patch shape.
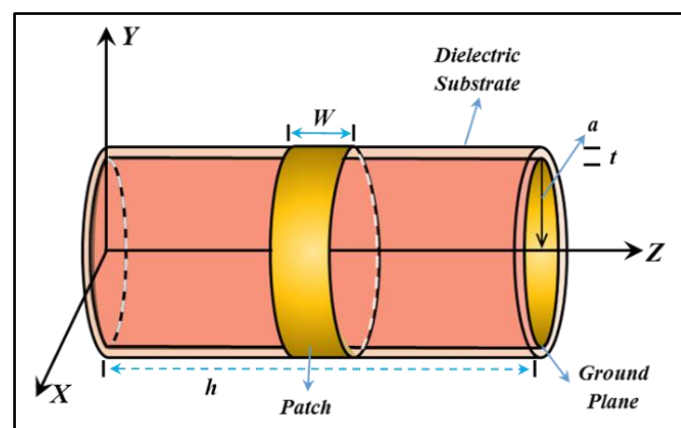


**Fig. 1**. Geometry of a single patch-antenna wraparound a dielectric-coated cylinder.

To find the radiation pattern issued by a wraparound microstrip antenna, the principle of equivalence is applied, which divides the antenna into an external valence region $[V^e]$ that includes the surface $S_{ce}$ (a surface separates the conductor with free space) and the surface $S_{de}$ (a surface separates the conductor and insulator) (9), see Fig. 2 (a). Moreover, Fig. 3(b) shows the diagram of the internal valence region $[V^d]$ that includes the surface $S_{de}$ and the surface $S_{cd}$ (surface separates both of the conductor and insulator).
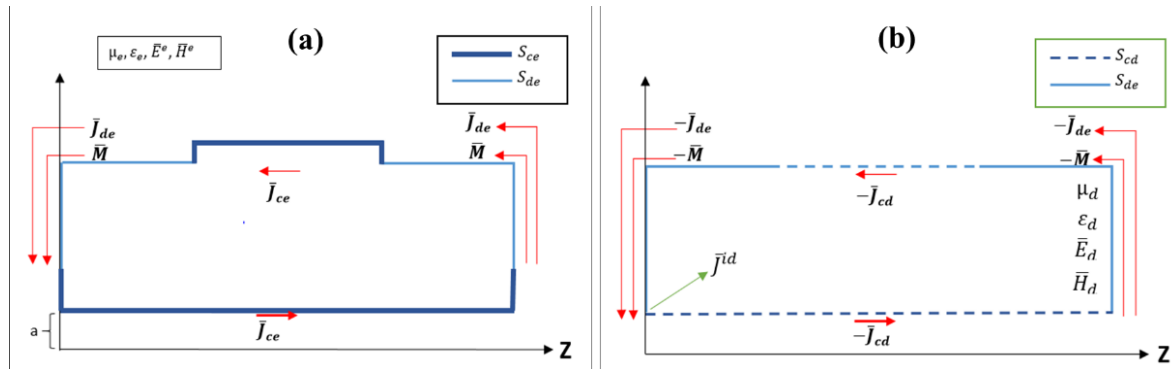


**Fig.** 2. Diagrams of: (a) External valence Region; and (b) Internal valence region

Using the equivalence principle that to replace the sources of the magnetic field with equivalent sources, which are surface currents can be written as(10):

$$\bar{J}_s = \hat{n} \times \bar{H}_s \tag{1}$$

$$\bar{M}_s = -\hat{n} \times \bar{E}_s \tag{2}$$

Since the antennas are made of conductive and conductive materials, there are two types of boundary conditions that assume the electric field's tangential components to the conducting surfaces, while the electric and magnetic field compounds remain constant on the insulating surfaces (11). These conditions are written as:

$$\hat{n} \times \bar{E}^e = 0 \qquad on\ S_{ce} \tag{3a}$$

$$\hat{n} \times \bar{E}^d = 0 \qquad on\ S_{cd} \tag{3b}$$

$$\hat{n} \times \bar{E}^d = \hat{n} \times \bar{E}^e \qquad on\ S_{de} \tag{3c}$$

$$\hat{n} \times \bar{H}^d = \hat{n} \times \bar{H}^e \qquad on\ S_{de} \tag{3d}$$

From these conditions, the density of surface currents can be obtained:

$$\bar{J}_{ce} = \hat{n} \times \bar{H}^e \qquad on\ S_{ce} \tag{4a}$$

$$\bar{J}_{cd} = \hat{n} \times \bar{H}^d \qquad on\ S_{cd} \tag{4b}$$

$$\bar{J}_{de} = \hat{n} \times \bar{H}^e \qquad on\ S_{de} \tag{4c}$$

$$\bar{M} = -\hat{n} \times \bar{E}^e \qquad on\ S_{de} \tag{4d}$$

Where $\bar{J}$ represents the electric current generated on the conducting surface and the dielectric. The magnetic current generated on the insulating surface, is denoted by $\bar{M}$. Thus, after applying the equivalence principle the integral equations can be written:

$$\hat{n} \times \bar{E}^e \left(\bar{J}_{ce} + \bar{J}_{de}, \bar{M}\right) = 0 \quad g \qquad\qquad on \ S_{ce} \qquad (5a)$$

$$\hat{n} \times \bar{H}^e \left(\bar{J}_{ce} + \bar{J}_{de}, \bar{M}\right) = 0 \qquad\qquad on \ S_{de} \qquad (5b)$$

$$\hat{n} \times \bar{E}^d \left(-\bar{J}_{cd} - \bar{J}_{de}, -\bar{M}\right) + \hat{n} \times \bar{E}^d\left(\bar{J}^{id}, 0\right) = 0 \quad j \quad on \ S_{cd} \qquad (5c)$$

$$\hat{n} \times \bar{H}^d \left(-\bar{J}_{cd} - \bar{J}_{de}, -\bar{M}\right) + \hat{n} \times \bar{H}^d\left(\bar{J}^{id}, 0\right) = 0 \quad m \quad on \ S_{de} \qquad (5d)$$

Where $\bar{E}^d\left(\bar{J}^{id}, 0\right)$ and $\bar{H}^d\left(\bar{J}^{id}, 0\right)$ are represented the electric and magnetic fields, resulting from the density of the feed current. Either $\bar{E}^e(\bar{J}, \bar{M})$, $\bar{H}^e(\bar{J}, \bar{M}), \bar{E}^d(\bar{J}, \bar{M}), \bar{H}^d(\bar{J}, \bar{M})$ denotes to the electric and magnetic fields, resulting from the equal currents $\bar{J}$ and $\bar{M}$.

The unknown quantities (equivalent surface currents) can be written as a function of the set of test functions using the trigonometric functions and the Fourier series, as:

$$\bar{J}_{ce} + \bar{J}_{de} = \sum_{n=-\infty}^{\infty}\left[\sum_{i=1}^{2(N-N_d-6)} I_{ni}^{1e}\bar{J}_{ni}^{1e} + \sum_{i=1}^{2(N_d-4)} I_{ni}\bar{J}_{ni}^{2e}\right] \qquad (6a)$$

$$\bar{J}_{cd} + \bar{J}_{de} = \sum_{n=-\infty}^{\infty}\left[\sum_{i=1}^{2(N-N_d-6)} I_{ni}^{1d}\bar{J}_{ni}^{1d} + \sum_{i=1}^{2(N_d-4)} I_{ni}\bar{J}_{ni}^{2d}\right] \qquad (6b)$$

$$\bar{M} = \eta_e \sum_{n=-\infty}^{\infty}\sum_{i=1}^{2(N_d-4)} k_{ni}\bar{M}_{ni} \qquad (6c)$$

When substituting equations (6) in equations (5), it is possible to obtain:

$$\sum_{n=-\infty}^{\infty}\left[\sum_{i=1}^{2(N-N_d-6)} I_{ni}^{1e}\bar{E}_{tan}^e(\bar{J}_{ni}^{1e}, 0) + \sum_{i=1}^{2(N_d-4)} I_{ni}\bar{E}_{tan}^e(\bar{J}_{ni}^{2e}, 0) + \eta_e \sum_{i=1}^{2(N_d-4)} k_{ni}\bar{E}_{tan}^e(0, \bar{M}_{ni})\right] = 0 \ on \ s_{ce} \quad (7a)$$

$$\sum_{n=-\infty}^{\infty}\left[\sum_{i=1}^{2(N-N_d-6)} I_{ni}^{1d}\bar{E}_{tan}^d(\bar{J}_{ni}^{1d}, 0) + \sum_{i=1}^{2(N_d-4)} I_{ni}\bar{E}_{tan}^d(\bar{J}_{ni}^{2d}, 0) + \eta_e \sum_{i=1}^{2(N_d-4)} k_{ni}\bar{E}_{tan}^d(0, \bar{M}_{ni})\right] = \bar{E}_{tan}^d(\bar{J}^{id}) \ on \ s_{cd} \quad (7b)$$

$$\sum_{n=-\infty}^{\infty}\left[\sum_{i=1}^{2(N-N_d-6)}\{I_{ni}^{1e}\bar{E}_{tan}^e(\bar{J}_{ni}^{1e}, 0) + I_{ni}^{1d}\bar{E}_{tan}^d(\bar{J}_{ni}^{1d}, 0)\} + \sum_{i=1}^{2(N_d-4)}\{I_{ni}\bar{E}_{tan}^e(\bar{J}_{ni}^{2e}, 0) + I_{ni}\bar{E}_{tan}^d(\bar{J}_{ni}^{2d}, 0)\} + \right.$$
$$\left.\eta_e \sum_{i=1}^{2(N_d-4)}\{k_{ni}\bar{E}_{tan}^e(0, \bar{M}_{ni}) + k_{ni}\bar{E}_{tan}^d(0, \bar{M}_{ni})\}\right] = \bar{E}_{tan}^d(\bar{J}^{id}) \qquad on \ S_{de} \qquad (7c)$$

$$\sum_{n=-\infty}^{\infty}\left[\sum_{i=1}^{2(N-N_d-6)}\{I_{ni}^{1e}\bar{H}_{tan}^e(\bar{J}_{ni}^{1e}, 0) + I_{ni}^{1d}\bar{H}_{tan}^d(\bar{J}_{ni}^{1d}, 0)\} + \sum_{i=1}^{2(N_d-4)}\{I_{ni}\bar{H}_{tan}^e(\bar{J}_{ni}^{2e}, 0) + I_{ni}\bar{H}_{tan}^d(\bar{J}_{ni}^{2d}, 0)\} + \right.$$
$$\left.\eta_e \sum_{i=1}^{2(N_d-4)}\{k_{ni}\bar{H}_{tan}^e(0, \bar{M}_{ni}) + k_{ni}\bar{H}_{tan}^d(0, \bar{M}_{ni})\}\right] = \bar{H}_{tan}^d(\bar{J}^{id}) \qquad on \ s_{de} \qquad (7d)$$

In this article the Galerkin technique is used, which states the weighting functions as a complex conjugate of the basic function (W=$J^*$) (12).

$$\bar{w}(\bar{r}) = \bar{w}^t(t, \emptyset) + \bar{w}^\emptyset(t, \emptyset) = \sum_{m=-\infty}^{\infty}\sum_{i=1}^{N-10}\left[\bar{w}_{mi}^t(t, \emptyset) + \bar{w}_{mi}^\emptyset(t, \emptyset)\right] \qquad (8a)$$

$$\bar{w}_{mi}^t(t, \emptyset) = \hat{u}_t f_i(t)e^{-jm\emptyset} \qquad\qquad \dots \quad (8b)$$

$$\bar{w}_{mi}^\emptyset(t, \emptyset) = \hat{u}_\emptyset f_i(t)e^{-jm\emptyset} \qquad\qquad \dots \ (8c)$$

Using the numerical multiplication of the weighting function with equations (7) that to obtain the following matrix form:

$$\begin{bmatrix} [Z_{ce,ce}^{1e}]_n & [0]_n & [Z_{ce,de}^{2e}]_n & \eta_e[Y_{ce,de}^{3e}]_n \\ [0]_n & [Z_{cd,cd}^{1d}]_n & [Z_{cd,de}^{2d}]_n & \eta_e[Y_{cd,de}^{3d}]_n \\ [Z_{de,ce}^{1e}]_n & [Z_{de,cd}^{1d}]_n & [Z_{de,de}^{2e} + Z_{de,de}^{2d}]_n & \eta_e[Y_{de,de}^{3e} + Y_{de,de}^{3d}]_n \\ [Y_{de,ce}^{1e}]_n & [Y_{de,cd}^{1d}]_n & [Y_{de,de}^{2e} + Y_{de,de}^{2d}]_n & \eta_e[Z_{de,de}^{3e} + Z_{de,de}^{3d}]_n \end{bmatrix}\begin{bmatrix} [I^{1e}]_n \\ [I^{1d}]_n \\ [I]_n \\ [K]_n \end{bmatrix} = \begin{bmatrix} [0]_n \\ [V_{cd}^d]_n \\ [V_{de}^d]_n \\ [I_{de}^d]_n \end{bmatrix} \quad \dots \quad (9)$$

Upon knowing the surface currents from the above equations, the relative fields in the far field can be calculated as follows (13):

$$E_\theta = \frac{-jw\mu_e}{4\pi r_\circ} e^{-jk_e r_\circ} F_1(\theta_\circ, \emptyset_\circ) \tag{10a}$$

$$E_\emptyset = \frac{-jw\mu_e}{4\pi r_\circ} e^{-jk_e r_\circ} F_2(\theta_\circ, \emptyset_\circ) \tag{10b}$$

$F_1$ and $F_2$ are known by the following equations:

$$F_1(\theta_\circ, \emptyset_\circ) = \int_s \left( \bar{J}(\bar{r}').\hat{\theta} + \frac{1}{\eta_e} \bar{M}(\bar{r}').\hat{\emptyset} \right) e^{-jk_e \hat{r}_\circ.\bar{r}'} ds \tag{11a}$$

$$F_2(\theta_\circ, \emptyset_\circ) = \int_s \left( \bar{J}(\bar{r}').\hat{\emptyset} - \frac{1}{\eta_e} \bar{M}(\bar{r}').\hat{\theta} \right) e^{-jk_e \hat{r}_\circ.\bar{r}'} ds \tag{11b}$$

$(r_\circ, \theta_\circ, \emptyset_\circ)$ is the vector units of a point in the far field.

## RESULTS AND DISCUSSION

In this study, to demonstrate the accuracy of a mathematical analysis for the proposed antenna and the correctness of the program used, a radiation result of single-patch wraparound antenna was compared with *L. Shafai* and *A. A. Kishk* (6). We note that there is good qualitative agreement between both numerical predication results, see Fig. 3. Typically, the radiation pattern of the basic magnetic plane (*H-plane*) plotted as a function of an azimuth angle $\theta$. Applying the numerical model presented above to solve the parameters of wraparound antenna that has been represented in Fig. 1, using a ground-plane radius as $a = 0.45\,\lambda$ and the length of the cylinder used is $h = 0.6\,\lambda$. In addition the patch width and dielectric-substrate thickness are $W = 0.328\,\lambda$ and $t = 0.02\,\lambda$, respectively. As can be seen in Fig. 3 the radiation pattern plotted as a function of azimuth angles, where the dielectric permittivity and frequency are $\epsilon_r = 2.32$ and 433 MHz respectively.
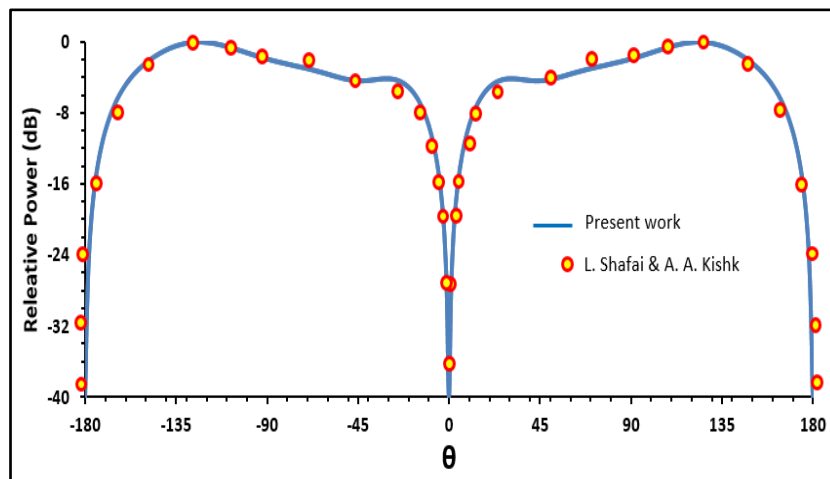


**Fig. 3.** Radiation pattern of single patch-antenna wraparound a dielectric-coated cylinder.

Since the wraparound the microstrip antenna is symmetric antenna, so there is symmetry in the voltage matrix when the tangent $V^t$ and axial $V^\emptyset$ are drawn for both the conducting surfaces $S_{ce}$ and $S_{cd}$ and the dielectric surface $S_{de}$ Fig. 4.
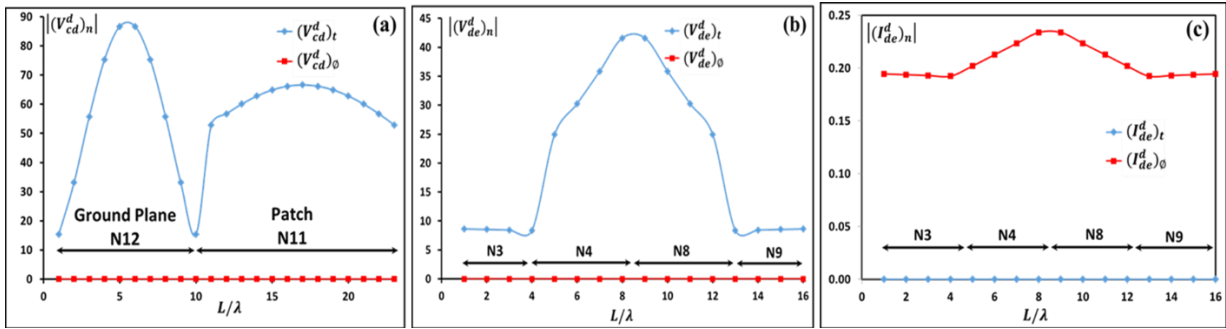
**Fig. 4.** Shows the numerical results of the secondary excitation matrices (a) $V_{cd}^t$ (b) $V_{de}^t$ and (c) $I_{de}^\emptyset$.

Fig. 5a shows the tangent $J^{dt}$ and axial $J^{d\emptyset}$ that diffuse on the inner surfaces of a wraparound microstrip antenna. Result shows the symmetry of the $S_{cd}$ and the $S_{de}$. While Fig. 5b shows the tangent $J^{et}$ and axial $J^{e\emptyset}$ of the density of the electric currents that propagate on the conductive external surfaces $S_{ce}$ and the dielectric $S_{de}$ of the antenna and through which radiation pattern are found in the far field. When the dominant zero modes are spread inside the antenna which in turn causes the axial $J^{e\emptyset}$ and axial $J^{d\emptyset}$ of zero value. However Fig. 5c represents the symmetry in the distribution of the axial $M^\emptyset$ on the external surface $S_{de}$, $M^t$ is zero value due to the spread of the zero mode.
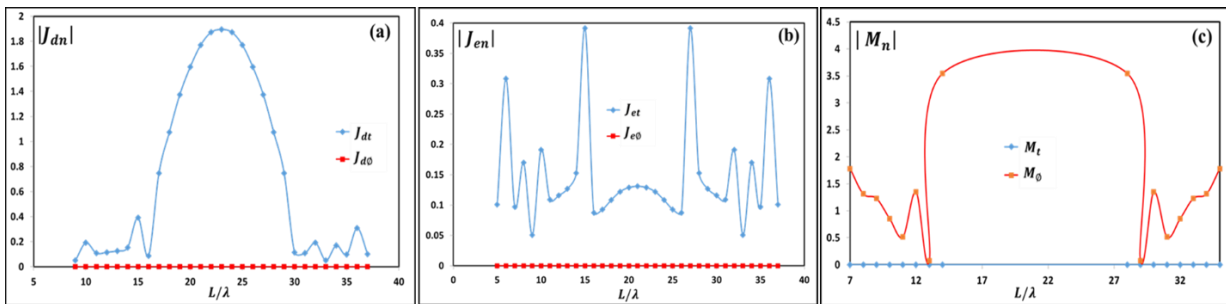


**Fig. 5**. Represents the density of the Electric $|J_n|$ and Magnetic $|M_n|$ currents that propagate on the outer and inner surfaces of wraparound microstrip antenna.

Thus, we can also analyze and measure more complex designs by adding more patches wraparound a dielectric-coated cylinder, see Fig. 6. In this step the interference for the scattering of radiation pattern from two-patch wraparound antenna have been predicted. The diagram of pair patch-antenna wraparound a dielectric-coated cylinder and the external with Internal valence regions, are clearly displayed in Fig. 6.
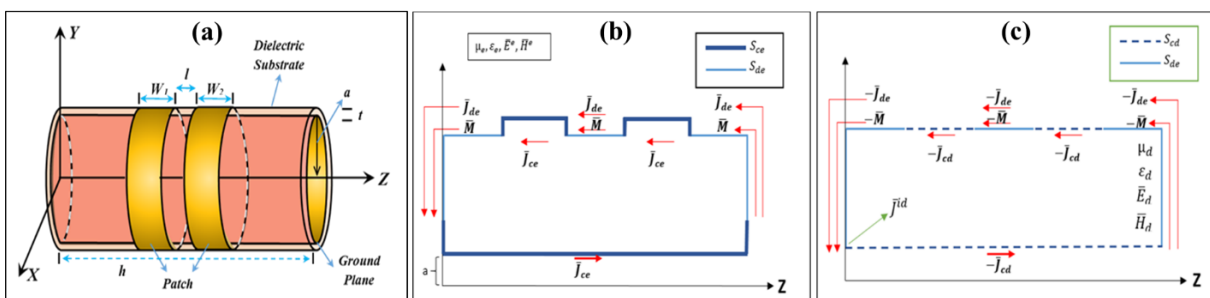


**Fig. 6.** Shows the diagrams of: (a) Dual patch-antenna wraparound a dielectric-coated cylinder (b) External valence Region; and (c) Internal valence region

Fig. 7 shows the comparison of *H-plane* radiation patterns are plotted for both a single and dual patch-antenna wraparound a dielectric-coated cylinder. The same electrical parameters were used in the above single patch-antenna, except for the patches width $W_1 = W_2 = 0.164\,\lambda$ and the separation distance between them $l = 0.07\,\lambda$. These predictions indicate that a good qualitative agreement with the numerical simulations, once again confirming the general validity of the model used to simulate these type of projects. As can be seen in Fig. 6, the radiation pattern for dual patch-antenna increased more than its value in the single patch-antenna. This is due to the resonant state between the two patches that creating an interference between for the surface currents generated on the antenna surfaces.
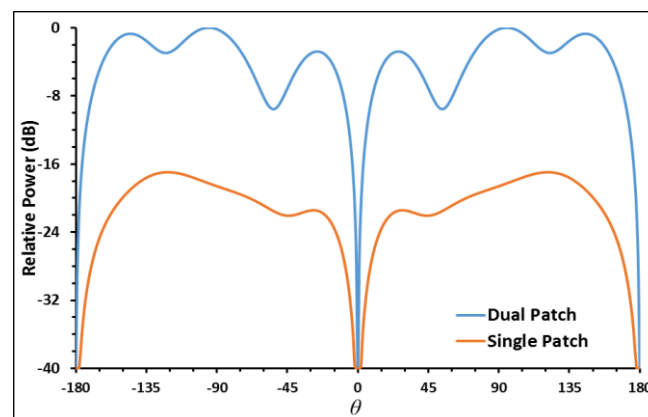


**Fig. 7.** Radiation pattern of a dual patch-antenna wraparound a dielectric-coated cylinder.

## CONCLUSION

The moment of method is a one of the important numerical methods for solving the body of revolution projects. In this paper, the differential and integral equations have been solved using Galerkin's technique. This model used to design a wraparound microstrip antenna and calculate its basic parameters such as the excitation matrices, the surface currents and also the radiation pattern. Numerical results show as a good qualitative agreement with previous studies, also with our suggested antenna. Which confirmed the general validity of the model used to simulate these type of projects. It is worth mentioning that the proposed antenna has a lot of applications, especially in the military equipment and air crafts.

### Acknowledgements

### Reference:

1. Das A, Das SK. Cylindrical transform technique for radiation pattern analysis of wraparound microstrip antenna on cylindrical body. IETE J Res. 1997;43(1):69–74.

2. Munson RE. Conformal Microstrip Atennas and Microstrip Phased Arrays. IEEE Trans Antennas Propag. 1974;AP-22(1):74–8.

3. de Assis FSB, Giarola AJ. Analysis of Microstrip Wraparound Antennas Using Dyadic Green's Functions. IEEE Trans Antennas Propag. 1983;31(2):248–53.

4.  Ventura TB, Pereira-Filho OMC, Do Rêgo CG. Cavity-backed cylindrical wraparound antennas. SBMO/IEEE MTT-S Int Microw Optoelectron Conf Proc. 2009;57–60.

5.  Soares AJM, Fonseca SBA, Giarola AJ. Space wave radiation efficiency of a wraparound antenna and the effect of surface wave radiation due to the dielectric substrate truncation. IEEE Trans Antennas Propag. 1990;38(6):934–8.

6.  James JR, Hall PS. Handbook of Microstrip Antennas, Peter Peregrinus Ltd. London) behalf IEE. 1989;1.

7.  Sensale-Rodriguez B, Sensale B, Leitao VMA, Peixeiro C. Microstrip antenna analysis using the method of fundamental solutions. Int J Numer Model Electron Networks, Devices Fields. 2008;21(6):563–81.

8.  Carter R. The Method of Moments in Electromagnetics, by W.C. Gibson. Contemp Phys. 2010;51(2):183–4.

9.  Kishk AA. Electromagnetic Scattering from Composite Objects Using a Mixture of Exact and Impedance Boundary Conditions. IEEE Trans Antennas Propag. 1991;39(6):826–33.

10. Shaaban RM, Ahmed ZA, Godaymi WA. Radiation Patterns Account of a Circular Microstrip Antenna Loaded Two Annular. J Nat Sci Res www.iiste.org ISSN. 2016;6(22):71–81.

11. Arvas E, Arabi AR, Sadigh A, Rao SM. Scattering from multiple conducting and dielectric bodies of arbitrary shape. IEEE Antennas Propag Mag. 1991;33(2):29–36.

12. Gouda M. The method of moment for the electromagnetic scattering from bodies of revolution. University of Borås/School of Engineering; 2009.

13. Yang C, Ruan YZ. Radiation characteristics of wraparound microstrip antenna on cylindrical body. Electron Lett. 1993;29(6):512–4.